Research Article | Vol. 12, No. 1 / 1 January 2021 / Biomedical Optics Express 480
Biomedical Optics EXPRESS

Label-free and noninvasive method for assessing the metabolic status in type 2 diabetic rats with myocardium diastolic dysfunction

KAI GUO,[1,5] JUNXIN WU,[2,5] YAWEI KONG,[2] LI ZHOU,[2] WEI LI,[1] YIYAN FEI,[2] JIONG MA,[2,3,4,6] AND LAN MI[2,7]

[1]*Department of Cardiology, Xinhua Hospital Affiliated to Shanghai Jiao Tong University School of Medicine, 1665 Kongjiang Road, Shanghai 200092, China*
[2]*Department of Optical Science and Engineering, Key Laboratory of Micro and Nano Photonic Structures (Ministry of Education), Shanghai Engineering Research Center of Ultra-Precision Optical Manufacturing, Green Photoelectron Platform, Fudan University, 220 Handan Road, Shanghai 200433, China*
[3]*Institute of Biomedical Engineering and Technology, Academy for Engineer and Technology, Fudan University, 220 Handan Road, Shanghai 200433, China*
[4]*The Multiscale Research Institute of Complex Systems (MRICS), School of Life Sciences, Fudan University, 220 Handan Road, Shanghai 200433, China*
[5]*These authors contributed equally to this work*
[6]*jiongma@fudan.edu.cn*
[7]*lanmi@fudan.edu.cn*

Abstract: This study assesses the metabolic status of rat diabetic cardiomyopathy (DCM) models. Echocardiography is used to detect the diastolic dysfunction in type 2 diabetic rats, and a lower threshold for inducible atrial fibrillation is found in type 2 diabetic rats with diastolic dysfunction compared to the control. Metabolic abnormalities are detected by status changes of reduced nicotinamide adenine dinucleotide (phosphate) (NAD(P)H), which is an essential coenzyme in cells or tissues. Fluorescence lifetime imaging microscopy (FLIM) is used to monitor changes in NAD(P)H in both myocardial tissues and blood. FLIM reveals that the protein-bound proportion of NAD(P)H in rat myocardium in the DCM group is smaller than the control group, which indicates the oxidative phosphorylation rate of the DCM group decreased. Similar results are found for blood plasma of DCM rats by the FLIM study. FLIM exhibits high potential for screening DCM as a label-free, sensitive, and noninvasive method.

1. Introduction

Diabetes is a chronic metabolic disease characterized by high blood glucose, and the International Diabetes Federation reported that the number of patients with diabetes worldwide had reached 463 million [1]. Increased blood glucose will gradually deteriorate the heart function, leading to cardiovascular disease and heart failure. Cardiovascular disease is the critical cause of death in patients with diabetes, and the risk of heart failure in patients with diabetes is 2–4 times those with normal blood glucose levels [2]. In 1972, Rubler first described diabetic cardiomyopathy (DCM), which is a disease of myocardial structure and function that is independent of hypertension, coronary heart disease, heart valve abnormalities, and other types of heart disease [3]. The main features are early metabolic disorders of myocardial cells, myocardial fibrosis, and microvascular disease, which cause structural abnormalities like left atrium enlargement and left ventricular hypertrophy, developing into diastolic dysfunction without contractile dysfunction [4]. DCM affects approximately 12% of people with diabetes and appears in some patients with well-controlled blood glucose [5,6].

Since the molecular mechanism of pathology has not been elucidated, there is currently no specific and effective diagnostic method of DCM. Clinical imaging technologies mainly

#413347 https://doi.org/10.1364/BOE.413347
Journal © 2021 Received 23 Oct 2020; revised 10 Dec 2020; accepted 11 Dec 2020; published 17 Dec 2020

Biomedical Optics EXPRESS

include echocardiography, magnetic resonance imaging (MRI), and positron emission computed tomography (PET). Echocardiography is used to detect changes in myocardial structure, valve, and blood flow velocity. It can detect diastolic dysfunction in the middle and late stages of DCM, but it is affected by the heart rate and angle during measurements [7–9]. MRI can assess left ventricular ejection fraction and contraction, myocardial mass, and fibrosis information, but may underestimate diastolic dysfunction, and MRI is incompatible with certain pacemakers or implantable defibrillators, which is not suitable for all patients [10,11]. To detect early metabolic disorders in the heart, PET needs to be injected with a radioactive developer fluorodeoxyglucose. Because of its radioactivity and the long time required for overall detection and analysis, it is rarely used in the early diagnosis of DCM [12,13]. Due to the limitations of current imaging technologies and the difficulty of detecting early metabolic disorders, it is essential to deeply study the pathogenesis of DCM and develop new diagnostic methods.

The endogenous biological fluorophores in cells and tissues mainly include reduced nicotinamide adenine dinucleotide (phosphate) (NAD(P)H) and flavin adenine dinucleotide (FAD), elastin, and collagen. NAD(P)H and FAD are important coenzymes involved in biological metabolism. FLIM can detect the metabolic status based on the fluorescence lifetime characteristics of endogenous coenzymes [14–16]. Studies have reported that NAD(P)H fluorescence lifetime can be used to assess the metabolic status of living cardiomyocytes cultured *in vitro* [17,18], and metabolism changes related to myocardial infarction and heart failure in rats [19]. FLIM was also used to detect intravascular images of atherosclerotic plaques in rabbits [20] and NAD(P)H images in an isolated perfused rat heart model [21]. In terms of blood glucose monitoring, variations of the glucose level of *in vitro* adipocytes were monitored by the auto-fluorescence lifetime [22,23]. Some other diseases caused by diabetes were studied by FLIM, such as diabetic nephropathy in frozen slice [24] and diabetic retinopathy patients by fundus autofluorescence [25]. So far, there is limited research on the metabolic state of DCM.

This work investigated the metabolic status by label-free FLIM on the myocardial tissues and blood plasma in a rat model of type 2 DCM, combined with the ultrasound electrocardiogram and electrophysiology study. A novel fast and noninvasive method for screening of DCM is proposed.

2. Materials and Methods

2.1. Zucker Diabetic Fatty Rat Model

The Zucker diabetic fatty (ZDF) rat is most widely used for studying type 2 diabetes (T2DM) associated with obesity. It has a missense mutation in the gene coding the leptin receptor (fa/fa) and spontaneously develops insulin resistance, T2DM, hyperlipidemia, moderate hypertension, and obesity, as well as progressive renal injury [26]. This rat strain possesses high reproductive efficiency and therefore should serve as a useful model of young- to middle-aged adult-onset type 2 diabetes in the studies of the pathophysiology, therapeutic interventions, and complications of the disease [27]. All animal experiments were approved by the Ethics Committee of Xinhua Hospital affiliated to Shanghai Jiao Tong University School of Medicine and were performed in compliance with the National Institutes of Health Guidelines for the care and use of laboratory animals. ZDF rats (n=9) were used as a model of diastolic dysfunction, and ZDF lean rats (n=7) served as controls. Nine-week-old ZDF diabetic (fa/fa) and ZDF lean (fa/+) male rats (Charles River) were purchased in batches, 3 pairs at a time, from Beijing Vital River Laboratory Animal Technologies Co. Ltd. (Chaoyang District, Beijing, China). They were allowed 2 weeks for adaption, and then examined in the following 12-24 weeks. Their blood glucose was monitored throughout the experiments.

Biomedical Optics EXPRESS

2.2. Echocardiography and electrophysiological Study

Transthoracic echocardiography (Vivid 7, GE Medical, Milwaukee, WI) was used to assess systolic and diastolic function in a blinded fashion. Rats were anesthetized with 2% isoflurane inhalation. To maintain the 37°C body temperature, the rats were placed on a heated pad. Parasternal short-axis views were used to record M-mode tracings at the left ventricular (LV) midpapillary level to measure LV dimensions, including LV anterior wall, LV posterior wall, ejection fraction, and fractional shortening. The apical 4-chamber view was used to assess the area of the left atrial (LA) at the end-ventricular systole. The apical 4-chamber view was also used to record pulse-wave Doppler mode and tissue Doppler mode tracing to evaluate the diastolic function. Measurements were performed at least three consecutive cardiac cycles under stable conditions.

Intracardiac electrophysiological (EP) studies, as described before [28], were conducted in a blinded fashion too. The rats were briefly anesthetized with 2% isoflurane inhalation. Surface electrocardiogram (ECG) and intracardiac electrogram were simultaneously recorded and analyzed by Lab Chart Software 7.0 (AD Instruments). An electrode catheter (1.1 F, Science) was advanced into the right atrium through the right jugular vein, and a burst of electrical stimuli was used to test the inducibility of atrial arrhythmias. Atrial fibrillation (AF) was induced by atrial burst pacing, starting with 5-s burst pacing at a cycle length of 50 ms and decreasing to 48, 46, 44, and 42 ms, and then shortened up to 10 ms in successive bursts. AF was defined as the occurrence of rapid, fragmented atrial electrocardiograms with irregular R-R intervals lasting ≥15 s.

2.3. Rat myocardium and blood plasma samples

Rats were anesthetized by an abdominal injection of sodium phenobarbital (100 mg/kg), and then venous blood samples were collected in vacuum collection tubes containing ethylenediaminetetraacetic acid (EDTA). The hearts were extracted, and part of the LA was longitudinally sectioned with a thickness of around 1 mm. The fresh tissues were preserved in phosphate-buffered saline (PBS) on ice for less than 3 h during the FLIM measurement study. The remaining part of rat hearts were fixed in 10% formalin overnight and embedded in paraffin. Subsequently, the LA and LV were sectioned with 5-μm thickness following standard protocols for pathologic examination (Fig. S1). Fresh blood samples were centrifuged to obtain blood plasma, and then the blood plasma smear samples on glass slides were analyzed by FLIM.

2.4. Microscope setup

The single-photon excitation FLIM (SP-FLIM) of fresh myocardial tissue and blood plasma samples was conducted using a time-correlated single-photon counting (TCSPC) system (SPC-150, Becker & Hickl, Germany) based on a laser scanning confocal microscope (Olympus FV300/IX71, Japan) equipped with a 60×W/NA=1.2 objective. The fluorescence signal was excited by a 405 nm picosecond laser (50 MHz, BDL-405-SMC, Becker & Hickl, Germany) and collected by a PMT (PMC-100-1, Becker & Hickl, Germany) through a 417–477 nm BP filter. Each image of 256 × 256 pixels was about 200 μm×200 μm. For each sample, at least five areas were imaged randomly.

The fresh rat myocardial tissues were also imaged by two-photon excitation FLIM (TP-FLIM) and second harmonic generation (SHG) using a Leica TCS SP8 DIVE FALCON microscope (Leica, Germany) equipped with a femtosecond (fs) pulsed laser (InSight X3 Dual, USA) and a 63×W/NA=1.2 objective. The autofluorescence of tissues was excited by the 810 nm fs pulsed laser and collected by a hybrid detector (HyD, Leica, Germany) through a 417–477 nm bandpass (BP) filter. The SHG signal was excited by the 850 nm fs pulsed laser and collected by a 420–430 BP filter.

Biomedical Optics EXPRESS

2.5. Microscopic images analysis

The FLIM data were analyzed with the double-exponential decay model by SPCImage software (Becker & Hickl, Berlin, Germany) for SP-FLIM and by LAS X software (Leica Microsystems, Germany) for TP-FLIM. To determine the fitting models, both the double-exponential and triple-exponential were assessed, with the fluorescence lifetime of free NAD(P)H (t_1) floating or fixed. When fixing t_1, the value was set at 460 ps according to the experimental result of free NADH solution measured by the FLIM setup. Moreover, the t_1 value was fixed due to the high conservatism of free state of NAD(P)H, as the various previous reports [29–31]. The comparison of double-exponential and triple-exponential with t_1 floating or fixed was shown in Fig. S2 and an example of different fitting functions was listed in Table S1. It was found that double-exponential function with t_1 fixed at 460 ps was better than others with the goodness-of-fit χ^2 values closer to one. Therefore, the average fluorescence lifetime was fitted by the double-exponential model as follows:

$$t_m = a_1 t_1 + a_2 t_2. \quad (1)$$

Where t_m is the mean lifetime, t_1 is the short fluorescence lifetime component and fixed at 460 ps, t_2 is the long fluorescence lifetime component, and a_1 and a_2 are the corresponding fractional contribution of the exponential component (a_1+a_2=1). t_2 is the fluorescence lifetime of protein-bound NAD(P)H, which varies according to the different bounded proteins. Since t_1 is fixed when fitting the double-exponential decay, t_2, a_2, as well as t_m can be calculated by minimizing the χ^2 value for a reasonable fit. After fitting, the t_2, a_2, or t_m distribution curve of all pixels in each FLIM image can be obtained by the SPCImage software, and the peak value of the curve was analyzed. P value was calculated by Student's t-test compared with control.

The quantifying colocalization analysis of FLIM and SHG images was calculated by the ImageJ software (National Institutes of Health, USA) to obtain Pearson's correlation coefficient (PCC) and Mander's colocalization coefficient (MCC) [32,33].

3. Results and discussion

3.1. Echocardiography and electrophysiological study

Consistent with the findings of DCM, ZDF diabetic rats showed diastolic dysfunction and preserved systolic function. Analysis of E'- and A'-wave changes in tissue Doppler revealed a decreased E'/A' ratio (Fig. 1(A)). The E'/A' ratio was 1.674 ± 0.269 in ZDF lean rats and 0.982 ± 0.265 in ZDF diabetic rats, $P < 0.05$. The E/A ratio was also decreased in pulse-wave Doppler (Fig. 1(B)). The E/A ratio was 1.809 ± 0.172 in ZDF lean rats and 1.304 ± 0.168 in ZDF diabetic rats, $P < 0.05$. The E/E' ratio was increased in ZDF diabetic rats (20.658 ± 3.167) compared with that in ZDF lean rats (16.860 ± 1.794), $P < 0.05$ (Fig. 1(C)). Atrial echocardiography confirmed the enlargement of the left atrial chamber in ZDF diabetic rats, which was 27.810 ± 3.585 mm^2, while the LA area was 18.532 ± 2.303 mm^2 in ZDF lean rats, $P < 0.05$ (Fig. 1(D)). However, the ejection fraction (EF%) was preserved in both groups (74.657 ± 2.368 in ZDF lean rats vs. 70.754 ± 4.969 in ZDF diabetic rats, $P > 0.05$) (Fig. 1(E)). The severity of diastolic dysfunction correlated with LA enlargement. Linear regression analyzed the relationship between LA size and diastolic dysfunction (Fig. 1(F)). Table S2 summarizes echocardiographic and anatomic measurements in the two groups. Cardiac hypertrophy was evident from the augmented heart weight, and the ratio of heart weight to body weight was (0.318 ± 0.002)% in ZDF lean rats and (0.329 ± 0.003)% in ZDF diabetic rats, although there was no significant difference. The histology of the hearts was shown in Fig. S1 and no significant difference was found.

To determine the effect of diastolic dysfunction on the vulnerability to AF, an overdrive atrial pacing protocol was performed on rats. As shown in Fig. 2, no AF was recorded in ZDF lean rats (0/6), whereas a remarkable increase was found in ZDF diabetic rats (4/6), P<0.05.

Biomedical Optics EXPRESS

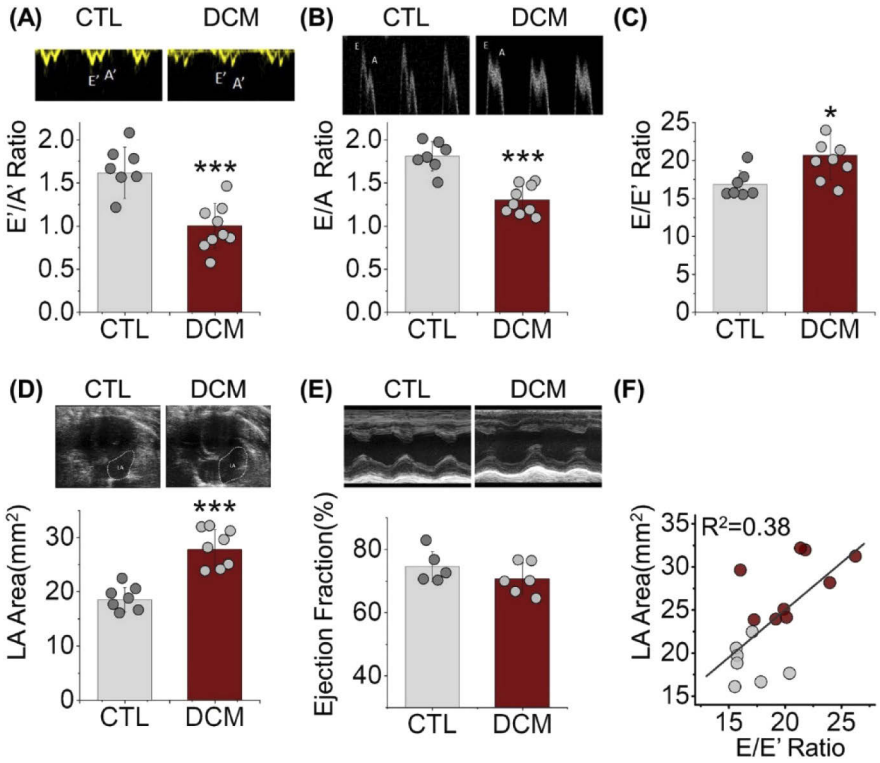

Fig. 1. Diastolic dysfunction was detected in ZDF diabetic rats. (A) Representative echocardiography images (top) of tissue Doppler describing E' and A' wave changes (bottom). (B) Representative images (top) of pulse-wave Doppler at the mitral level showing E (early filling) and A (atrial filling) wave changes (bottom). (C) E/E' ratio of ZDF diabetic rats was increased compared with ZDF lean rats. (D) Representative recordings (top) and quantification of the LA area (bottom). (E) Representative M-mode of parasternal short-axis views (top) of ejection fraction analysis (bottom). (F) Relationship between E/E' ratio and LA area, data fit by linear regression. n = 5–7 in ZDF lean rats, and n = 6–9 in ZDF diabetic rats. *P<0.05 vs. control group.

3.2. *Microscopy observation of myocardial tissues of rats*

To investigate the sources of autofluorescence in myocardial tissues, the combination of TP-FLIM and SHG imaging was used. The SHG requires medium with non-central symmetry, mainly structural proteins such as collagen, microtubules and muscle myosin [34,35]. It has been demonstrated that the endogenous fluorophores in cells and tissues display different emission spectra, with NAD(P)H peaking at 450 nm, FAD peaking at 550 nm, collagen at 390 nm and elastin at 410 nm [36]. TP-FLIM with a 417–477 nm BP filter in this work can obtain autofluorescence signals, mainly from NAD(P)H, and partly from collagen and elastin. While SHG signal of myocardial tissues mainly from collagen as previously reported [34,37–39]. FLIM (Fig. 3(A)) and SHG (Fig. 3(B)) displayed the structural patterns of the fresh myocardium tissue from a LA. Figure 3(C) shows an overlay image. As marked by the arrows, the black oval indicated by arrow 1 is a myocardial cell nucleus with a weak fluorescent signal, and the blue oval area marked by arrow 2 is a red blood cell. Arrow 3 pointed to the myocardial reverse striation. PCC and MCC can effectively evaluate the degree of correlation and colocalization between two images [32,33]. The PCC value close to 1 indicates correlated objects. The MCC values, M1 and M2, represent the overlap ratio of one signal to the other. The PCC value between Figs. 3(A) and

Biomedical Optics EXPRESS

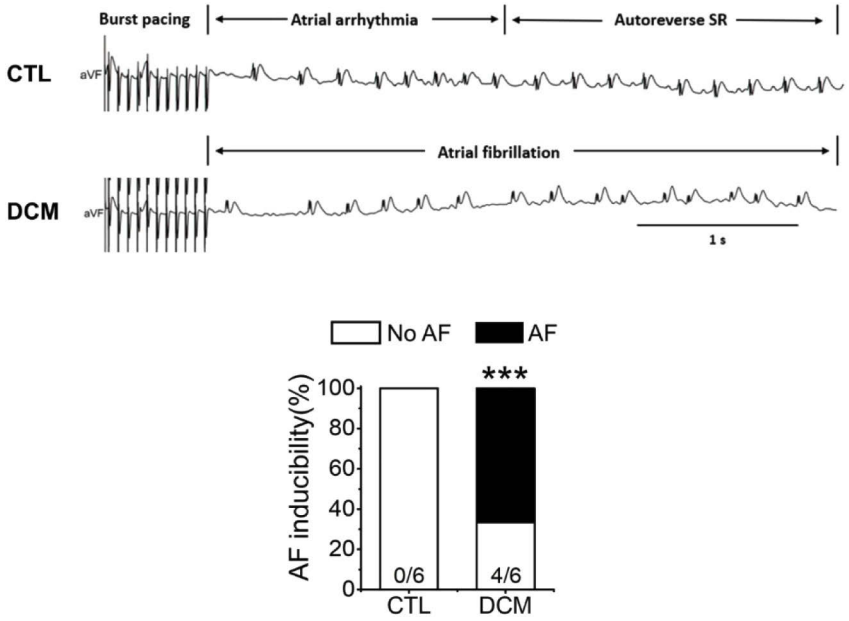

Fig. 2. Increased AF incidence in ZDF diabetic rats. Representative recordings of surface ECG (lead aVF) for ZDF lean rats (top) and ZDF diabetic rats (bottom). n = 6 in each group. *P<0.05 vs. control group.

3(B) was -0.08, which indicates a low correlation between FLIM and SHG signals in myocardial tissues. MCC calculations indicate that 2% of the autofluorescence localizes with SHG and 75% of SHG signal localizes with autofluorescence. It is noticeable that the fluorescence and SHG signals of myocardial tissue partially colocalized, which was also observed in cardiac tissues of a murine model [40] and porcine hearts [37]. Of the various endogenous fluorophores, the collagen and elastin are related to the structure of tissues, while only NAD(P)H relates to the metabolic status. Since the histology of the heart tissues showed no detectable difference between DCM and control as shown in Fig. S1, the fluorescence lifetime change of rat myocardial tissue is mainly from coenzyme NAD(P)H, which can reflect the metabolic state.

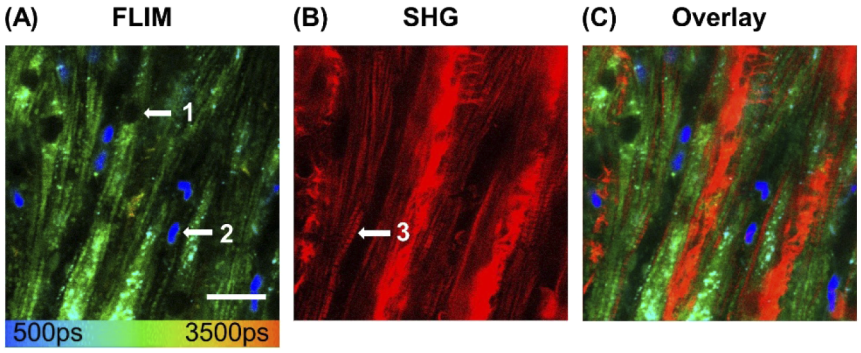

Fig. 3. Representative TP-FLIM (A) and SHG (B) images of the myocardium tissue from a rat left atrium. Arrows 1, 2, and 3 point to a myocardial cell nucleus, a red blood cell, and myocardial reverse striations, respectively. The overlay image (C) showed partial colocalization of fluorescence signal and SHG signal (Scale bar is 20 μm).

Biomedical Optics EXPRESS

SP-FLIM can produce images with higher fluorescence quantum yield than TP-PLIM. In addition, the excitation source of SP-FLIM is a picosecond pulsed laser with moderate cost. The following FLIM images of fresh myocardial tissue slices and blood plasma samples were all observed by SP-FLIM. Figure 4 exhibited the representative FLIM images of myocardial tissues. A large number of parallel cardiomyocytes were displayed in orange in Figs. 4(B) and 4(E), indicating that the average lifetime t_m of cardiomyocytes was similar in the control group and DCM group. There was a network of long average lifetime structures (displayed in blue) in Figs. 4(B) and 4(E) with the diameter about 1-2.5 μm, which might be collagen fibrils or bundles of fibrils [41–43]. For the control group, t_m showed differences between the left and right parts in Fig. 4(B). However, there was no significant difference in the corresponding distribution image (Fig. 4(C)) of protein-bound NAD(P)H proportion (a_2). As shown in Fig. 4(C), the a_2 image of the two parts was similar in bluish-green (the orange oval area pointed by the white arrow is a red blood cell). It indicated that the protein-bound state of NAD(P)H in different areas of the control group were similar. In Fig. 4(F), it can be seen that the myocardial tissue of the DCM rat shows different characteristics from the control group; that is, the a_2 value of myocardial cells was smaller than those of the control group. This implies that myocardial cells mainly accounted for the abnormal metabolism of the myocardium in DCM rats instead of fibrils. Figure 4(G) shows the t_m distribution curves of Figs. 4(B) and 4(E). The t_m peak of the control group is 1027 ± 2 ps, and that of the group with diabetes is 898 ± 3 ps, which is slightly shorter than the control group. Figure 4(H) shows the a_2 distribution curves of Figs. 4(C) and 4(F), showing the a_2 peak of the control group at 32.2 ± 1.3%, and the a_2 peak of the diabetes group decreasing to 23.6 ± 0.2%. Figures 4(I) and 4(H) show the statistical analysis of t_m and a_2 in rat myocardial tissues for the DCM group and the control group (6 rats were studied in each group). The average blood glucose of the control group was 5.3 ± 0.4 mM, and that of the DCM group was 19.5 ± 3.2 mM. As blood glucose increased, the proportion of protein-bound NAD(P)H decreased. The average a_2 of the control group was 37.0 ± 3.0%, and that of the DCM group was 32.1 ± 2.0%. The lifetime of protein-bound NAD(P)H (t_2) was also analyzed for the DCM and control groups, as shown in Fig. S3. The bound-NAD(P)H lifetime ranged from 2.0 to 3.5 ns, and no detectable difference of t_2 was found between the DCM and control groups.

3.3. Measuring blood plasma samples of rats with FILM

To further investigate the metabolic interrelation between the myocardial tissues and blood samples, the blood plasma of rats was smeared on glass and measured by SP-FLIM. The average fluorescence lifetime (t_m) of the control group was 1376 ± 71 ps, and that of the diabetes group was 990 ± 50 ps. Figures 5(A) and 5(B) show the FLIM a_2 images of rat blood plasma, in which the peak of the control group at 39.4 ± 0.4% was more significant than that of the diabetes group at 24.4 ± 0.4% (Fig. 5(C)). The trend of a_2 of the two blood plasma samples was consistent with the results of myocardial tissues. Figure 5(D) shows the statistical data of the NAD(P)H a_2 in rat blood plasma. The difference between the control group and the DCM group was significant ($P<0.01$), with 36.1 ± 1.5% for the control group and 23.2 ± 1.9% for the DCM group.

3.4. Discussion

Patients with DM with a specific impairment of the heart muscle, independent of vascular defects, and hypertension have DCM. Cardiomyopathy is also found in the rodent models of both type 1 [44] and type 2 [45] DM. The ZDF rat, which is widely used for studying T2DM, is characterized by development of diabetes between 7 and 12 weeks of age, which reaches 100% incidence at around 20 weeks of age [26,27]. Since rodents are resistant to atherosclerosis, these models provide strong evidence for the occurrence of DCM [46]. The changes in cardiac structure and function are the main clinical manifestation of DCM. In this sense, echocardiography is traditionally used to diagnose DCM. Using echocardiography, many clinical studies confirm left

Biomedical Optics EXPRESS

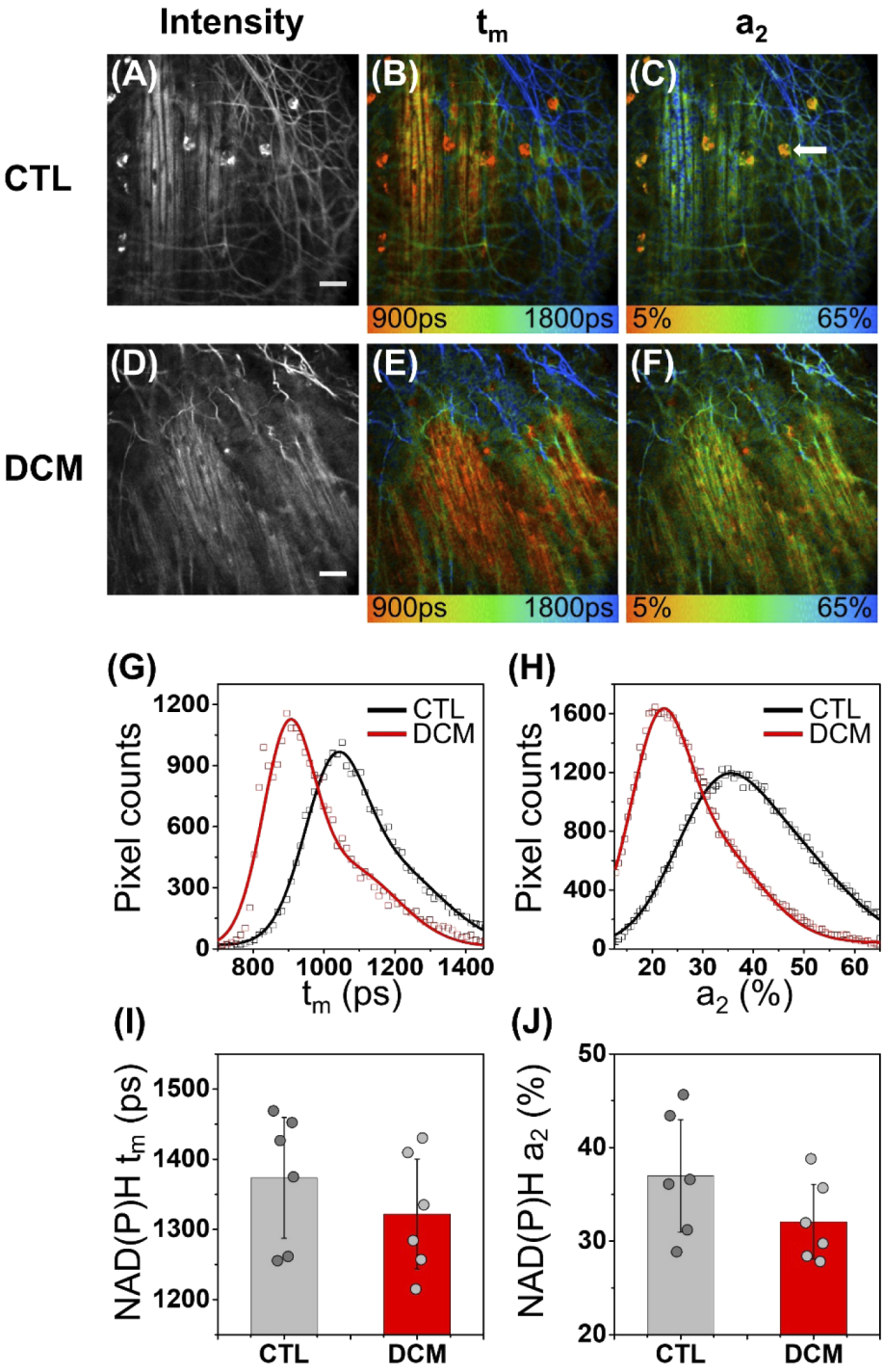

Fig. 4. (A)-(F) Representative FLIM images of myocardial tissues from rat left atriums of CTL (control) group and DCM group. The three columns are the fluorescence intensity images, the average fluorescence lifetime (t_m) distribution images, and the proportion of protein-bound NAD(P)H (a_2) images. (Scale bar is 20 μm.) (G)-(H) The corresponding t_m and a_2 distribution curves of FLIM images of control and DCM. (I)-(J) The average NAD(P)H t_m and a_2 of rats' myocardial tissues (n = 6 in each group).

Biomedical Optics EXPRESS

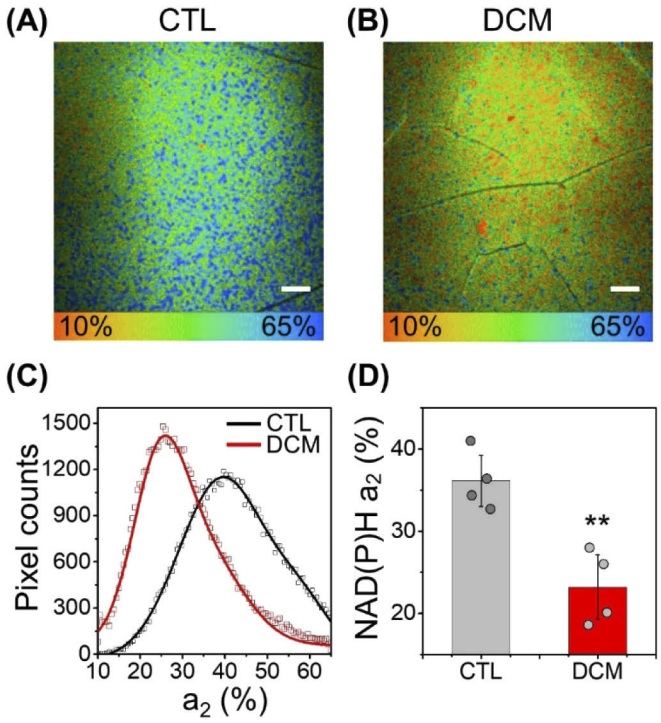

Fig. 5. The FLIM a_2 (protein-bound NAD(P)H proportion) images of blood plasma for control (A) and DCM (B) (Scale bar is 20 μm). (C) The corresponding distribution curves of images A and B. (D) The average NAD(P)H a_2 of blood plasma of rats (n = 4 in each group, ** P<0.01 vs. control group).

ventricular hypertrophy (LVH) in patients with DM and even in people with impaired glucose tolerance [47,48]. In this study, the ratio of heart weight to body weight was higher in ZDF diabetic rats than in ZDF lean rats. Accordingly, the thickness of the left ventricle wall was greater in ZDF diabetic rats. Using pulse-wave and tissue Doppler, a decreased E/A ratio and increased E/E' ratio were found in ZDF diabetic rats, which confirmed the presence of diastolic dysfunction. Another character of DCM is atrial enlargement. The LA serves as a reservoir during ventricular systole, as a conduit during early diastole, and as an active contractile chamber that augments LV filling in late diastole. Studies have shown that changes in LA size and function were associated with adverse clinical events such as atrial fibrillation, stroke, diastolic dysfunction and LV failure [49]. The importance of LA enlargement has been established in the guidelines about assessment of LV diastolic function [50]. Clinical studies showed that LA volume and function in patients with T2DM were independent predictors of cardiovascular events, such as the high prevalence of atrial fibrillation and heart failure [51,52]. Furthermore, impaired LA function may be present in patients with newly diagnosed T2DM [49]. Our experimental results were consistent with these findings. The echocardiography test showed a larger LA in ZDF diabetic rats, and their vulnerability to AF was increased during in vivo EP studies. All this myocardium remodeling, including LVH, diastolic dysfunction, and atrial enlargement, confirmed that metabolic disorders play an essential role in the pathophysiology of DCM. Therefore, an effective technique to test the myocardial metabolism will be optimal for DCM diagnosis.

Fatty acid (FA) oxidation accounts for 60% of the energy provided by the normal adult heart, and the remaining 40% is provided by glucose and other fuels [53]. Compared with normal hearts, the hearts of patients with diabetes are accustomed to over-oxidizing glucose and reduced

Biomedical Optics EXPRESS

glycolysis and pyruvate oxidation [54,55]. Mitochondrial FA oxidation is the main NADH producer in the diabetic heart. The increased use of cardiac FA in asymptomatic of patients with diabetes suggests that changes in mitochondrial metabolism precede the changes in cardiology [56]. The acetyl-CoA is mainly generated by the oxidation of FA and glucose in the myocardium. Then, acetyl-CoA enters the tricarboxylic acid (TCA) cycle, consuming NAD+ and producing increased NADH [57]. In addition, the electron transport chain defects in the diabetic heart will further increase NADH. Thus, we propose a label-free and noninvasive method to monitor the metabolic changes of DCM by measuring the NAD(P)H status of the myocardium and blood plasma.

The reduction of a_2 revealed a change along the metabolic trajectory, from protein-bound NAD(P)H to free NAD(P)H. The increased free/bound NAD(P)H ratio could be resulted from complex conditions, such as a metabolic shift from oxidative phosphorylation to glycolysis and the oxidative/reductive stress. As previously reported, the mitochondrial oxidative phosphorylation rate of atrial tissue in type 2 diabetes patients was reduced [54]. The electron transport chain had defects, causing a decrease in the ratio of NAD(P)+/NAD(P)H in mitochondria, as well as the increased proportion of free NAD(P)H. A mechanism of increased oxidative stress in the diabetic heart was reported [58]. However, in contrast to the general consensus, Berthiaume *et al.* proposed that a reductive redox stress may precede and induce the observed oxidative stress in DCM [57]. Moreover, various studies observed reduced free/bound NAD(P)H ratio by phasor FLIM or time-resolved fluorescence spectroscopy when oxidative stress was induced in living cells [59,60]. Nevertheless, the key mechanism remains to be elucidated. In this study, FLIM was used to test the metabolic status in the LA and blood by NAD(P)H fluorescence characteristics. In ZDF diabetic rats, the a_2 values of LA were smaller than those in ZDF lean rats, much like the a_2 values of blood. Though to determine the origin of NAD(P)H in blood is difficult, there are several reports attributed the blood plasma emission mainly to NAD(P)H. For instance, Madhuri *et al.* observed the primary emission peak around 460 nm with 405 nm excitation for human blood plasma and attributed it to enzyme-bound NAD(P)H [61]. Similar autofluorescence characteristics was also reported for blood plasma of diabetic rats [62] and blood plasma of malignant melanoma patients when excited by UV light [63], and both of them have attributed the emission to NADH. In recent years, NADH was found a sensor of local blood-flow need [64]. NAD has also been recognized as an extracellular signal molecule and can be released from neurons in blood vessels [65]. The NAD concentrations in both blood and tissues were found lower in quinolinic acid phosphoribosyltransferase knockout mice when niacin deficient [66]. Although it is not clear that the specific relationship between NAD(P)H in blood and that in myocardial tissue, it is reasonable to believe that myocardial metabolism changes accordingly with metabolic micro-environment, which is reflected by blood metabolism. Further studies should be conducted to reveal the source of blood NAD(P)H and the underlying mechanisms.

It is important to measure the metabolic status within an appropriate period of time. In the present work, the samples were *ex vivo* heart tissues with PBS preservation on ice for less than 3 h, where the NAD(P)H autofluorescence signal must be affected by the extraction of hearts compared with *in vivo*, as the recent report on the *ex vivo* and *in vivo* rat liver tissue samples [31]. Rodimova *et al.* reported that the metabolic state of hepatocytes did not change within 3 h [31]. Schenke-Layland *et al.* observed substantial ultrastructural deterioration and disintegration of most collagenous structures in cryopreserved tissues compared with fresh tissues [67]. For cells and tissues, fixation and mounting have different effect on the autofluorescence of NAD(P)H. Poulon *et al.* observed the fluorescence lifetimes of NADH and FAD in fixed samples were longer than those of fresh samples [68]. Wang *et al.* demonstrated that the fluorescence lifetime of NADH was enhanced immediately by paraformaldehyde then remain steady for at least 14 days in neutral balsam for HeLa and A549 cells [69]. So it is necessary to keep the same extraction

Biomedical Optics EXPRESS

procedure, the preservation media, the fixation and period when comparing the metabolic status for fixed cells or tissues.

4. Conclusions

We conducted a FLIM study on the unstained myocardial tissue and blood plasma of ZDF diabetic rats. TP-FLIM and SHG imaging revealed that the dominant source of autofluorescence of myocardium is NAD(P)H, which can be used to monitor the metabolic status by FLIM. It was found that the proportion of protein-bound NAD(P)H in myocardial tissue and blood plasma decreased in a rat DCM model. This was tested by echocardiography, and diastolic dysfunction was found. Furthermore, the electrophysiology study showed that DCM rats with diastolic dysfunction were more likely to induce AF. Hyperglycemia decreased metabolic efficiency with the decline of oxidative phosphorylation proportion. It indicated that the oxidative phosphorylation rate decreased along with the diastolic dysfunction. Therefore, FLIM provides valuable information about myocardial metabolism, and it may be used as a noninvasive, label-free, and rapid method for the early detect responses of DCM, forecasting hypertrophy, diastolic dysfunction, or even susceptibility of AF.

Funding

National Natural Science Foundation of China (81770321); Fudan University (FC2017-007, FC2018-001); Academy for Engineering and Technology, Fudan University (gyy2018-001, gyy2018-002).

Disclosures

The authors declare no conflicts of interest.

See Supplement 1 for supporting content.

References

1. International Diabetes Federation, "IDF Diabetes Atlas 2019," https://www.diabetesatlas.org/en/resources/.
2. G. Borghetti, D. von Lewinski, D. M. Eaton, H. Sourij, S. R. Houser, and M. Wallner, "Diabetic cardiomyopathy: current and future therapies. beyond glycemic control," Front. Physiol. **9**, 1514 (2018).
3. S. Rubler, J. Dlugash, Y. Z. Yuceoglu, T. Kumral, A. W. Branwood, and A. Grishman, "New type of cardiomyopathy associated with diabetic glomerulosclerosis," The Am. J. Cardiol. **30**(6), 595–602 (1972).
4. A. P. Lourenco, A. F. Leite-Moreira, J. L. Balligand, J. Bauersachs, D. Dawson, R. A. de Boer, L. J. de Windt, I. Falcao-Pires, R. Fontes-Carvalho, S. Franz, M. Giacca, D. Hilfiker-Kleiner, E. Hirsch, C. Maack, M. Mayr, B. Pieske, T. Thum, C. G. Tocchetti, D. L. Brutsaert, and S. Heymans, "An integrative translational approach to study heart failure with preserved ejection fraction: a position paper from the Working Group on Myocardial Function of the European Society of Cardiology," Eur. J. Heart Fail. **20**(2), 216–227 (2018).
5. A. Lorenzo-Almoros, J. Tunon, M. Orejas, M. Cortes, J. Egido, and O. Lorenzo, "Diagnostic approaches for diabetic cardiomyopathy," Cardiovasc. Diabetol. **16**(1), 28 (2017).
6. T. Konstantinos and S. Sideris, "Diabetic cardiomyopathy: from pathophysiology to treatment," Hellenic J. Cardiol. **55**(5), 411–421 (2014).
7. V. C. Patil, H. V. Patil, K. B. Shah, J. D. Vasani, and P. Shetty, "Diastolic dysfunction in asymptomatic type 2 diabetes mellitus with normal systolic function," J. Cardiovasc. Dis. Res. **2**(4), 213–222 (2011).
8. J. Mori, V. B. Patel, O. Abo Alrob, R. Basu, T. Altamimi, J. Desaulniers, C. S. Wagg, Z. Kassiri, G. D. Lopaschuk, and G. Y. Oudit, "Angiotensin 1-7 ameliorates diabetic cardiomyopathy and diastolic dysfunction in db/db mice by reducing lipotoxicity and inflammation," Circ. Heart Fail. **7**(2), 327–339 (2014).
9. M. M. Lima-Martinez, M. Paoli, M. Rodney, N. Balladares, M. Contreras, L. D'Marco, and G. Iacobellis, "Effect of sitagliptin on epicardial fat thickness in subjects with type 2 diabetes and obesity: a pilot study," Endocrine **51**(3), 448–455 (2016).
10. G. Korosoglou and P. M. Humpert, "Non-invasive diagnostic imaging techniques as a window into the diabetic heart: a review of experimental and clinical data," Exp. Clin. Endocrinol Diabetes **115**(4), 211–220 (2007).

Biomedical Optics EXPRESS

11. C. Jellis, J. Wright, D. Kennedy, J. Sacre, C. Jenkins, B. Haluska, J. Martin, J. Fenwick, and T. H. Marwick, "Association of imaging markers of myocardial fibrosis with metabolic and functional disturbances in early diabetic cardiomyopathy," Circ. Cardiovasc. Imaging **4**(6), 693–702 (2011).
12. L. J. Rijzewijk, R. W. van der Meer, H. J. Lamb, H. W. de Jong, M. Lubberink, J. A. Romijn, J. J. Bax, A. de Roos, J. W. Twisk, R. J. Heine, A. A. Lammertsma, J. W. Smit, and M. Diamant, "Altered myocardial substrate metabolism and decreased diastolic function in nonischemic human diabetic cardiomyopathy: studies with cardiac positron emission tomography and magnetic resonance imaging," J. Am. Coll Cardiol. **54**(16), 1524–1532 (2009).
13. X. Palomer, J. Pizarro-Delgado, and M. Vazquez-Carrera, "Emerging actors in diabetic cardiomyopathy: heartbreaker biomarkers or therapeutic targets?" Trends Pharmacol. Sci. **39**(5), 452–467 (2018).
14. Q. Yu and A. A. Heikal, "Two-photon autofluorescence dynamics imaging reveals sensitivity of intracellular NADH concentration and conformation to cell physiology at the single-cell level," J. Photochem. Photobiol. B **95**(1), 46–57 (2009).
15. M. C. Skala, K. M. Riching, D. K. Bird, A. Gendron-Fitzpatrick, J. Eickhoff, K. W. Eliceiri, P. J. Keely, and N. Ramanujam, "In vivo multiphoton fluorescence lifetime imaging of protein-bound and free nicotinamide adenine dinucleotide in normal and precancerous epithelia," J. Biomed. Opt. **12**(2), 024014 (2007).
16. H. Li, J. Yu, R. Zhang, X. Li, and W. Zheng, "Two-photon excitation fluorescence lifetime imaging microscopy: A promising diagnostic tool for digestive tract tumors," J. Innovative Opt. Health Sci. **12**(5), 1930009 (2019).
17. Y. Cheng, M. Ren, Y. Niu, J. Qiao, S. Aneba, D. Chorvat Jr., and A. Chorvatova, "Assessment of mitochondrial metabolic oxidative state in living cardiomyocytes with spectrally-resolved fluorescence lifetime spectroscopy of NAD(P)H," Sheng Wu Yi Xue Gong Cheng Xue Za Zhi. **26**(6), 1191–1200 (2009).
18. A. Chorvatova, A. Mateasik, and D. Chorvat Jr, "Spectral decomposition of NAD(P)H fluorescence components recorded by multi-wavelength fluorescence lifetime spectroscopy in living cardiac cells," Laser Phys. Lett. **10**(12), 125703 (2013).
19. J. Lagarto, B. T. Dyer, C. Talbot, M. B. Sikkel, N. S. Peters, P. M. French, A. R. Lyon, and C. Dunsby, "Application of time-resolved autofluorescence to label-free in vivo optical mapping of changes in tissue matrix and metabolism associated with myocardial infarction and heart failure," Biomed. Opt. Express **6**(2), 324–346 (2015).
20. M. W. Lee, J. W. Song, W. J. Kang, H. S. Nam, T. S. Kim, S. Kim, W. Y. Oh, J. W. Kim, and H. Yoo, "Comprehensive intravascular imaging of atherosclerotic plaque in vivo using optical coherence tomography and fluorescence lifetime imaging," Sci. Rep. **8**(1), 14561 (2018).
21. J. L. Lagarto, B. T. Dyer, C. B. Talbot, N. S. Peters, P. M. W. French, A. R. Lyon, and C. Dunsby, "Characterization of NAD(P)H and FAD autofluorescence signatures in a Langendorff isolated-perfused rat heart model," Biomed. Opt. Express **9**(10), 4961–4978 (2018).
22. N. D. Evans, L. Gnudi, O. J. Rolinski, D. J. Birch, and J. C. Pickup, "Glucose-dependent changes in NAD(P)H-related fluorescence lifetime of adipocytes and fibroblasts in vitro: potential for non-invasive glucose sensing in diabetes mellitus," J. Photochem. Photobiol. B **80**(2), 122–129 (2005).
23. J. C. Pickup, F. Hussain, N. D. Evans, O. J. Rolinski, and D. J. Birch, "Fluorescence-based glucose sensors," Biosens. Bioelectron. **20**(12), 2555–2565 (2005).
24. S. Ranjit, K. Henriksen, A. Dvornikov, M. Delsante, A. Rosenberg, M. Levi, and E. Gratton, "Phasor approach to autofluorescence lifetime imaging FLIM can be a quantitative biomarker of chronic renal parenchymal injury," Kidney Int. **98**(5), 1341–1346 (2020).
25. D. Schweitzer, L. Deutsch, M. Klemm, S. Jentsch, M. Hammer, J. Dawczynski, and U. A. Mueller, "Detection Of early metabolic alterations in diabetes mellitus by time-resolved fundus autofluorescence (FLIM)," Invest. Ophthalmol. Visual Sci. **52**(14), 1753 (2011).
26. B. L. Leonard, R. N. Watson, K. M. Loomes, A. R. Phillips, and G. J. Cooper, "Insulin resistance in the Zucker diabetic fatty rat: a metabolic characterisation of obese and lean phenotypes," Acta Diabetol. **42**(4), 162–170 (2005).
27. N. Yokoi, M. Hoshino, S. Hidaka, E. Yoshida, M. Beppu, R. Hoshikawa, K. Sudo, A. Kawada, S. Takagi, and S. Seino, "A Novel Rat Model of Type 2 Diabetes: The Zucker Fatty Diabetes Mellitus ZFDM Rat," J. Diabetes Res. **2013**, 1–9 (2013).
28. Q. Wang, Y. Chen, D. Zhang, C. Li, X. Chen, J. Hou, Y. Fei, Y. Wang, and Y. Li, "Activin Receptor-Like Kinase 4 Haplodeficiency Mitigates Arrhythmogenic Atrial Remodeling and Vulnerability to Atrial Fibrillation in Cardiac Pathological Hypertrophy," J. Am. Heart Assoc. **7**(16), e008842 (2018).
29. M. Zanello, F. Poulon, J. Pallud, P. Varlet, H. Hamzeh, G. Abi Lahoud, F. Andreiuolo, A. Ibrahim, M. Pages, F. Chretien, F. Di Rocco, E. Dezamis, F. Nataf, B. Turak, B. Devaux, and D. Abi Haidar, "Multimodal optical analysis discriminates freshly extracted human sample of gliomas, metastases and meningiomas from their appropriate controls," Sci. Rep. **7**, 41724 (2017).
30. A. Periasamy, P. T. C. So, K. König, X. S. Xie, M. M. Lukina, V. Dudenkova, A. V. Shumilova, L. B. Snopova, E. V. Zagaynova, and M. V. Shirmanova, "In vivo metabolic imaging of mouse tumor models in response to chemotherapy," Proc. SPIE **10069**, 100692G (2017).
31. S. Rodimova, D. Kuznetsova, N. Bobrov, V. Elagin, V. Shcheslavskiy, V. Zagainov, and E. Zagaynova, "Mapping metabolism of liver tissue using two-photon FLIM," Biomed. Opt. Express **11**(8), 4458–4470 (2020).
32. K. W. Dunn, M. M. Kamocka, and J. H. McDonald, "A practical guide to evaluating colocalization in biological microscopy," Am. J. Physiol. Cell Physiol. **300**(4), C723–C742 (2011).

Biomedical Optics EXPRESS

33. A. K. Miri, H. K. Heris, U. Tripathy, P. W. Wiseman, and L. Mongeau, "Microstructural characterization of vocal folds toward a strain-energy model of collagen remodeling," Acta Biomater. **9**(8), 7957–7967 (2013).
34. P. J. Campagnola and L. M. Loew, "Second-harmonic imaging microscopy for visualizing biomolecular arrays in cells, tissues and organisms," Nat. Biotechnol. **21**(11), 1356–1360 (2003).
35. P. J. Campagnola, A. C. Millard, M. Terasaki, P. E. Hoppe, C. J. Malone, and W. A. Mohler, "Three-dimensional high-resolution second-harmonic generation imaging of endogenous structural proteins in biological tissues," Biophys. J. **82**(1), 493–508 (2002).
36. M. S. Roberts, Y. Dancik, T. W. Prow, C. A. Thorling, L. L. Lin, J. E. Grice, T. A. Robertson, K. Konig, and W. Becker, "Non-invasive imaging of skin physiology and percutaneous penetration using fluorescence spectral and lifetime imaging with multiphoton and confocal microscopy," Eur. J. Pharm Biopharm. **77**(3), 469–488 (2011).
37. K. Konig, K. Schenke-Layland, I. Riemann, and U. A. Stock, "Multiphoton autofluorescence imaging of intratissue elastic fibers," Biomaterials **26**(5), 495–500 (2005).
38. R. Cicchi, D. Kapsokalyvas, V. De Giorgi, V. Maio, A. Van Wiechen, D. Massi, T. Lotti, and F. S. Pavone, "Scoring of collagen organization in healthy and diseased human dermis by multiphoton microscopy," J. Biophotonics **3**(1-2), 34–43 (2009).
39. H. G. Breunig, H. Studier, and K. Konig, "Multiphoton excitation characteristics of cellular fluorophores of human skin in vivo," Opt. Express **18**(8), 7857–7871 (2010).
40. C. J. Goergen, H. H. Chen, S. Sakadzic, V. J. Srinivasan, and D. E. Sosnovik, "Microstructural characterization of myocardial infarction with optical coherence tractography and two-photon microscopy," Physiol Rep. **4**(18), e12894 (2016).
41. M. K. O'Connell, S. Murthy, S. Phan, C. Xu, J. Buchanan, R. Spilker, R. L. Dalman, C. K. Zarins, W. Denk, and C. A. Taylor, "The three-dimensional micro- and nanostructure of the aortic medial lamellar unit measured using 3D confocal and electron microscopy imaging," Matrix Biol. **27**(3), 171–181 (2008).
42. P. Fratzl, *Collagen* (Springer, 2008).
43. R. Cicchi, N. Vogler, D. Kapsokalyvas, B. Dietzek, J. Popp, and F. S. Pavone, "From molecular structure to tissue architecture: collagen organization probed by SHG microscopy," J. Biophotonics **6**(2), 129–142 (2013).
44. J. J. Luiken, S. L. Coort, D. P. Koonen, D. J. van der Horst, A. Bonen, A. Zorzano, and J. F. Glatz, "Regulation of cardiac long-chain fatty acid and glucose uptake by translocation of substrate transporters," Pflugers Arch. **448**(1), 1–15 (2004).
45. E. Aasum, D. D. Belke, D. L. Severson, R. A. Riemersma, M. Cooper, M. Andreassen, and T. S. Larsen, "Cardiac function and metabolism in Type 2 diabetic mice after treatment with BM 17.0744, a novel PPAR-α activator," Am. J. Physiol. Heart Circ. Physiol. **283**(3), H949–H957 (2002).
46. A. Wan and B. Rodrigues, "Endothelial cell-cardiomyocyte crosstalk in diabetic cardiomyopathy," Cardiovasc. Res. **111**(3), 172–183 (2016).
47. M. K. Rutter, H. Parise, and E. J. Benjamin, "Impact of glucose intolerance and insulin resistance on cardiac structure and function. sex-related differences in the Framingham heart study," ACC Curr. J. Rev. **12**(3), 34–35 (2003).
48. A. J. M. Brown, C. Lang, R. McCrimmon, and A. Struthers, "Does dapagliflozin regress left ventricular hypertrophy in patients with type 2 diabetes? A prospective, double-blind, randomised, placebo-controlled study," BMC Cardiovasc. Disord. **17**(1), 229 (2017).
49. O. Gulmez, H. Parildar, O. Cigerli, and N. Demirag, "Assessment of left atrial function in patients with type 2 diabetes mellitus with a disease duration of six months," Cardiovasc. J. Afr. **29**(2), 82–87 (2018).
50. B. Pieske, C. Tschope, R. A. de Boer, A. G. Fraser, S. D. Anker, E. Donal, F. Edelmann, M. Fu, M. Guazzi, C. S. P. Lam, P. Lancellotti, V. Melenovsky, D. A. Morris, E. Nagel, E. Pieske-Kraigher, P. Ponikowski, S. D. Solomon, R. S. Vasan, F. H. Rutten, A. A. Voors, F. Ruschitzka, W. J. Paulus, P. Seferovic, and G. Filippatos, "How to diagnose heart failure with preserved ejection fraction: the HFA-PEFF diagnostic algorithm: a consensus recommendation from the Heart Failure Association (HFA) of the European Society of Cardiology (ESC)," Eur. J. Heart Fail. **22**(3), 391–412 (2020).
51. R. C. Serban and A. Scridon, "Data linking diabetes mellitus and atrial fibrillation-how strong is the evidence? From epidemiology and pathophysiology to therapeutic implications," Can. J. Cardiol. **34**(11), 1492–1502 (2018).
52. L. J. Bohne, D. Johnson, R. A. Rose, S. B. Wilton, and A. M. Gillis, "The association between diabetes mellitus and atrial fibrillation: clinical and mechanistic insights," Front. Physiol. **10**, 135 (2019).
53. K. A. De Jong and G. D. Lopaschuk, "Complex energy metabolic changes in heart failure with preserved ejection fraction and heart failure with reduced ejection fraction," Can. J. Cardiol. **33**(7), 860–871 (2017).
54. E. J. Anderson, A. P. Kypson, E. Rodriguez, C. A. Anderson, E. J. Lehr, and P. D. Neufer, "Substrate-specific derangements in mitochondrial metabolism and redox balance in the atrium of the type 2 diabetic human heart," J. Am. Coll Cardiol. **54**(20), 1891–1898 (2009).
55. S. Sankaralingam, O. A. Alrob, L. Zhang, J. S. Jaswal, C. S. Wagg, A. Fukushima, D. E. Johnstone, A. M. Sharma, and G. D. Lopaschuk, "Lowering body weight in obese mice with diastolic heart failure improves cardiac insulin sensitivity and function: implications for the obesity paradox," Diabetes **64**(5), 1643–1657 (2015).
56. P. Herrero, L. R. Peterson, J. B. McGill, S. Matthew, D. Lesniak, C. Dence, and R. J. Gropler, "Increased myocardial fatty acid metabolism in patients with type 1 diabetes mellitus," J. Am. Coll Cardiol. **47**(3), 598–604 (2006).
57. J. M. Berthiaume, J. G. Kurdys, D. M. Muntean, and M. G. Rosca, "Mitochondrial NAD(+)/NADH redox state and diabetic cardiomyopathy," Antioxid Redox Signal **30**(3), 375–398 (2019).

Biomedical Optics EXPRESS

58. H. Nakamura, S. Matoba, E. Iwai-Kanai, M. Kimata, A. Hoshino, M. Nakaoka, M. Katamura, Y. Okawa, M. Ariyoshi, Y. Mita, K. Ikeda, M. Okigaki, S. Adachi, H. Tanaka, T. Takamatsu, and H. Matsubara, "p53 promotes cardiac dysfunction in diabetic mellitus caused by excessive mitochondrial respiration-mediated reactive oxygen species generation and lipid accumulation," Cir. Heart Fail. **5**(1), 106–115 (2012).
59. C. Stringari, J. L. Nourse, L. A. Flanagan, and E. Gratton, "Phasor fluorescence lifetime microscopy of free and protein-bound NADH reveals neural stem cell differentiation potential," PLoS One **7**(11), e48014 (2012).
60. A. Chorvatova, S. Aneba, A. Mateasik, D. Chorvat Jr., and B. Comte, "Time-resolved fluorescence spectroscopy investigation of the effect of 4-hydroxynonenal on endogenous NAD(P)H in living cardiac myocytes," J. Biomed. Opt. **18**(6), 067009 (2013).
61. S. Madhuri, N. Vengadesan, P. Aruna, D. Koteeswaran, P. Venkatesan, and S. Ganesan, "Native fluorescence spectroscopy of blood plasma in the characterization of oral malignancy," Photochem. Photobiol. **78**(2), 197–204 (2003).
62. E. Shirshin, O. Cherkasova, T. Tikhonova, E. Berlovskaya, A. Priezzhev, and V. Fadeev, "Native fluorescence spectroscopy of blood plasma of rats with experimental diabetes: identifying fingerprints of glucose-related metabolic pathways," J. Biomed. Opt. **20**(5), 051033 (2015).
63. I. Spakova, M. Rabajdova, K. Dubayova, V. Nagyova, M. B. Pilatova, and M. Marekova, "Development of novel parameter for monitoring of malignant melanoma progression," Pract Lab Med. **22**, e00182 (2020).
64. Y. Ido, K. Chang, T. A. Woolsey, and J. R. Williamson, "NADH: sensor of blood flow need in brain, muscle, and other tissues," FASEB J. **15**(8), 1419–1421 (2001).
65. L. M. Smyth, J. Bobalova, M. G. Mendoza, C. Lew, and V. N. Mutafova-Yambolieva, "Release of beta-nicotinamide adenine dinucleotide upon stimulation of postganglionic nerve terminals in blood vessels and urinary bladder," J. Biol Chem. **279**(47), 48893–48903 (2004).
66. M. Terakata, T. Fukuwatari, M. Sano, N. Nakao, R. Sasaki, S. Fukuoka, and K. Shibata, "Establishment of true niacin deficiency in quinolinic acid phosphoribosyltransferase knockout mice," J. Nutr. **142**(12), 2148–2153 (2012).
67. K. Schenke-Layland, I. Riemann, O. Damour, U. A. Stock, and K. Konig, "Two-photon microscopes and in vivo multiphoton tomographs–powerful diagnostic tools for tissue engineering and drug delivery," Adv. Drug Deliv. Rev. **58**(7), 878–896 (2006).
68. F. Poulon, M. Zanello, A. Ibrahim, A. J. Zaylaa, and D. A. Haidar, "Comparison between fresh and fixed human biopsies using spectral and lifetime measurements: fluorescence analysis using one and two photon excitations," in *Proceedings of IEEE Conference on International Conference on Advances in Biomedical Engineering* (2015).
69. X. Wang, Y. Xie, M. Huang, L. Yao, Y. Wang, Y. Fei, J. Ma, and L. Mi, "Effect of fixation and mounting on fluorescence lifetime of cellular autofluorescence," IEEE J. Sel. Top. Quantum Electron. **25**(1), 1–6 (2019).